

## Elucidating the Interplay Between Entropy-Driven and Patch-Mediated Bonding in Directing Nanoscale Assemblies

Journal:	Molecular Systems Design & Engineering	
Manuscript ID	ME-ART-09-2024-000153.R1	
Article Type:	Paper	
Date Submitted by the Author:	16-Oct-2024	
Complete List of Authors:	Akkunuri, Kireeti; Johns Hopkins University, Chemical and Biomolecular Engineering Zhang, Xiangyu; Johns Hopkins University, Chemical and Biomolecular Engineering Vo, Thi; Johns Hopkins University, Chemical and Biomolecular Engineering	

SCHOLARONE™ Manuscripts

# Elucidating the Interplay Between Entropy-Driven and Patch-Mediated Bonding in Directing Nanoscale Assemblies

Kireeti Akkunuri<sup>1†</sup>, Xiangyu Zhang<sup>1†</sup>, Thi Vo<sup>1\*</sup>

- <sup>1</sup> Chemical and Biomolecular Engineering, Johns Hopkins University, Baltimore, MD 21218
- † Equal contributions
- \* Corresponding Author: tvo12@jhu.edu

## Design, System, Application Statement

Nanoscale building blocks with selective polymer surface patterning represent a class of materials with unprecedented degree of programmability in spatial and orientational orderings. There "patchy" nanoparticles blend the toughness and optical properties of inorganic particles with the flexibility and reconfigurability of polymeric patches, providing a route for fabricating chiral and/or low-coordination multifunctional materials with immediate applications in cargo encapsulation, membrane filtration, sensing, and or optical computing devices. However, due to the similarity in length scales between polymeric patches and the nanoparticle cores, grand challenges in their a priori design lie in a lack of fundamental understanding of how the interplay between flexible patchy interactions and entropic forces associated with particle geometries ultimately influence their hierarchical, mesoscale morphologies. In this work, we combine theory and simulation to explicitly quantify the interplay between enthalpic and entropic forces governing interactions between nanoparticles with flexible patches. We show that these nanoscale-level interactions readily propagate to the mesoscale and present a predictive theoretical framework that can rigorously quantify such effects. Our theory shows that precision engineering of polymeric patchy interactions can produce a diverse suite of symmetry-breaking interactions between nanoparticles, opening newer avenues for designing hybrid organic-inorganic metamaterials.

## **Elucidating the Interplay Between Entropy-Driven and Patch-Mediated Bonding in Directing Nanoscale Assemblies**

Kireeti Akkunuri<sup>1†</sup>, Xiangyu Zhang<sup>1†</sup>, Thi Vo<sup>1\*</sup>

<sup>1</sup> Chemical and Biomolecular Engineering, Johns Hopkins University, Baltimore, MD 21218

† Equal contributions

\* Corresponding Author: tvo12@jhu.edu

#### Abstract

Selective nanoparticle surface patterning presents incredible promise for broadening programmable materials design into a space beyond "close-packed" morphologies. These "patchy" particles impose directional attractions between neighbors that favor the formation of lowcoordination, open structures previously inaccessible via their isotropically interacting nanoparticle counterparts. However, unlike patchy colloids, patches on nanoparticles are highly deformable, presenting challenges for their predictive design. Here, we present a multi-faceted approach combining theory and simulation to investigate the underlying forces governing interactions between nanoparticles with flexible patches. We first develop a thermodynamic perturbation theory to fundamentally capture the interplay between patch-patch merging and directional entropic forces in controlling particle organization. We then employ theoretical insights to explicitly consider how monomer geometry synergizes with monomer connectivity in sculpting the equilibrium morphologies for polymeric chains composed of anisotropic monomeric subunits. Theory predictions are then validated using simulations, with excellent agreement across both local and global length scales. Combined, our findings indicate that a large suite of orientational and structural diversity can be attained via precision engineering of how patch-patch and entropic forces between the anisotropic nanoparticles counterbalance each other. These findings on nanoscale patchy interactions offer newer avenues for directing the assembly process of novel polymeric and metamaterials.

**Keywords:** self-assembly, nanoparticle, polymer, theory, molecular simulation

#### Introduction

Recent advances in nanoscale synthesis have resulted in a novel class of polymer functionalized nanoparticles (NPs) exhibiting patch-formation and symmetry breaking surface patterning<sup>1–5</sup>. Such "patchy" NPs impose specific spatial and orientational interactions relative to their neighboring particles that disfavor "close-packed" configurations, producing complex and/or low-coordination NP structural orderings<sup>6–16</sup>. Typical morphologies include the formation of porous superlattices<sup>8–12,14</sup>, host-guest configurations<sup>15–20</sup>, and/or chiral supramolecular motifs<sup>21–23</sup> – all of which are of interest as they exhibit macroscopic properties ideal for modern day applications. For example, host-guest and/or porous lattices exhibit tunability in cavity sizes, relevant for cargo encapsulation and filtration-based transport processes. Similarly, chiral superstructures exhibit unique optical/photonic responses that make them amenable for use in sensing and optical computing devices. Combined, these findings have enabled access to tunable, open-lattice morphologies using nanoscale synthetic building blocks, expanding both the space of their programmable complexity beyond "close-packed" morphologies as well as their potential for application in previously inaccessible fields<sup>4,24–27</sup>.

A grand challenge hindering the inverse design of patchy, anisotropic NP assemblies, however, lies in understanding how patch-patch interactions between NPs influence their equilibrium spatial and orientational configurations. Unlike colloids whose patch thicknesses are small relative to particle size<sup>13,28–32</sup>, NPs possess patch thicknesses with sizes similar to their insphere radius<sup>1,3</sup>. This difference in thickness results in patch-patch interactions that are significantly more rigid for colloids as compared to NPs. In fact, recent experimental findings have revealed that patch-patch interactions produce "bonds" between NPs that can twist, relax, and dynamically reconfigure on the seconds timescale<sup>33</sup>, in contrast to the hours to days relaxation times observed for colloids<sup>34,35</sup>. In short, patchy NP interactions are highly flexible and exhibit bond-like rotational behaviors. This means that predictions of patch-mediated NP assemblies must balance the interplay between entropic forces due to shape anisotropy and NP-NP connectivity resulting from the flexible "bonds" that arise between patch merging.

Through this lens, bonding interactions between patchy NPs are reminiscent of flexible polymers, suggesting that ideas from polymer physics can be employed to provide insights into their equilibrium behaviors. While preliminary works from the polymers community have elucidated the role of anisotropic, ribbon-like monomers on chain conformations<sup>36</sup>, a generalized

framework capable of accounting for arbitrarily shaped monomer geometries remains elusive. Here, we present one framework capable of predicting the equilibrium spatial and orientational behaviors for systems of anisotropic NPs that accounts for both entropic and bonding interactions. Specifically, we generalize the idea of entropic forces between anisotropic particles<sup>37</sup> to account for bonding constraints between different locations on the NP surface, reflecting the high degree of molecular patterning currently accessible in experimental systems<sup>4,5</sup>. We then employ our framework to develop a scaling theory that accurately predicts equilibrium chain statistics for systems of polymeric NPs connected via patch-patch merging, validated using simulations. Furthermore, we apply our results to predict previously reported behaviors of patchy triangular prism<sup>33</sup> and polymeric "bundlemers" in the literature, showcasing our theory's generalizability to experimentally relevant systems. Our work not only provides a fundamental understanding of the underlying forces governing patchy, anisotropic NP interactions, but also presents a generalization of polymer theory to consider the effect of monomer geometry on chain conformations. The former serves as a critical step for inverse design of patchy NP assemblies while the latter generalizes predictions for polymer conformations to complex systems containing polyhedrally shaped (POSS, carborane, fullerene), conjugated, and/or aromatic monomers<sup>39</sup>.

### Theory

Shape Anisotropy and Entropic Bonding Theory (EBT). To capture the interplay between inter-NP connectivity and directional entropic forces resulting from particle geometry, we propose a generalization of entropic bonding theory<sup>37</sup> (EBT). Here, it is instructive to describe the fundamental concepts of the original theory. Briefly, EBT quantifies the local excluded volume between neighboring NPs to compute their free energy of interactions. Excluded volume quantification employs the *ansatz* of pseudoparticles (pPs) to define a mean-field interaction potential (Eq. 1) between NPs and pPs that is then coupled with the Smoluchowski equation (Eq. 2) to solve for the free energy (E) of a given set of NP configuration<sup>37</sup>:

$$\beta U_m(r) = r^{-2} \left[ \ln \rho_{pP}(r) - \beta \mu_{pP} \right] + \sum_{i}^{N} \beta U_{core}(r)$$
 (1)

$$\left[\nabla^2 + \beta \nabla^2 U_m - (\beta \nabla U_m)^2\right] \rho_{pp} = E \rho_{pp} \tag{2}$$

where r defines the pP-NP center-to-center separation,  $\rho_{pP}$  and  $\mu_{pP}$  are the density distribution and chemical potential of pPs, respectively, and  $\beta = 1/kT$ .  $U_{core}(r)$  represents a hard-core

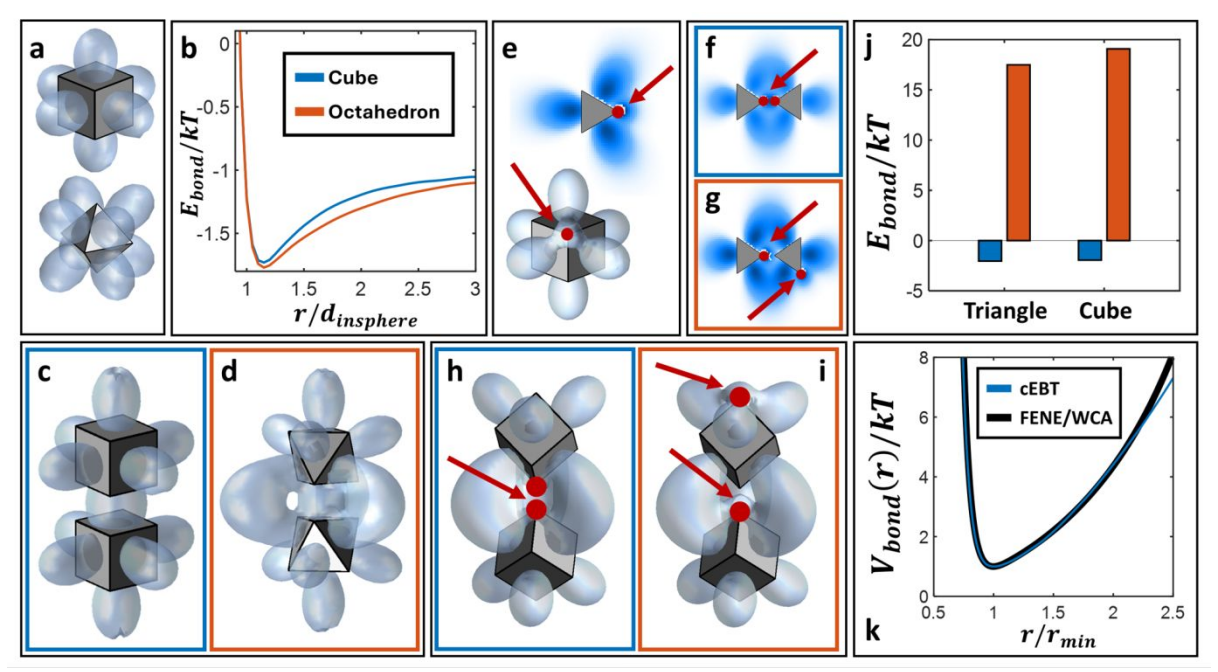


Figure 1. Connectivity-Generalization for Entropic Bonding Theory (cEBT). Shape orbitals for a) cube and octahedron from EBT. b) Entropic bond potential ( $E_{bond}$ ) from EBT between pairs of cubes and octahedra. r is the center-to-center distance and  $d_{insphere}$  is the insphere diameter of each shape. Visualization of the optimal orientations and relative center-to-center spacing between the particles for c) cubes and d) octahedra reveals that orbital overlap drives energy minimization. Shape orbitals for e) 2D patchy triangle and 3D patchy cube using cEBT. cEBT calculations for pairs of triangles with the same relative orientation, but with f) aligned versus g) misaligned bonds reveal shifts in the pP equilibrium distributions. h) and i) show analogous bond alignment versus misalignment for patchy cubes. j) Predicted cEBT bonding energy between aligned (blue) vs misaligned (orange) configurations. k) Comparison of bonding potential predicted from cEBT and a FENE-WCA bond indicate an analogous functional form between both potentials. Red dots and arrows indicate the bonding sites.

repulsion between each NP and all pPs to prevent particle overlaps. Note that Eq. 1 defines the single reference NP limit. To generalize to multiple NPs,  $\rho_{pP}$  is constructed by summing over pP densities about each individual NP within the system. Furthermore, solutions to Eqs. 1 – 2 take advantage of change of variables into the coordinate spaces commensurate with particle geometries to define "shape harmonics" for NPs (Fig. 1a). In the case of spherical NPs, these shape harmonics are identical to the well-known spherical harmonics obtained as solutions to the homogenous, zero-potential form of Eq. 2 (i.e.  $\nabla^2 \rho_{pP} = 0$ ). For this reason, when coupled with its corresponding radial solutions, such shape harmonics are defined as "shape orbitals" in analogy to the correspondence between spherical harmonics and atomic orbitals from quantum mechanics (QM). Through the lens of EBT, shape orbitals provide a metric for direct quantification of the

emergent directional interactions between NPs. Maximization of shape orbital overlaps between neighboring NPs minimizes their free energy of interaction to produce an "entropic bond," analogous to how atomic orbital overlaps in QM drive covalent bond formation. An example of the minimization of the free energy ( $E_{bond}$ ) between two neighboring cubes and two neighboring octahedra using EBT is shown in **Fig. 1b-d.** Note that the higher orbital overlap between octahedra produces both longer range and a net lower free energy. For its full derivation, we refer the reader to the original publication on EBT<sup>37</sup>.

Connectivity-Generalization of Entropic Bonding Theory (cEBT). To bridge the predictive capabilities of EBT to systems of connected, anisotropic NPs, we first note that shape orbitals (Fig. 1a) are plots of  $\rho_{pP}$ , which are the general solutions for the pP distribution from Eqs. 1 – 2. By definition,  $\rho_{pP}$ , therefore, quantifies the local excluded volume imposed from the reference NP on its neighbors. Our connectivity-generalization to EBT (cEBT) assumes that connectivity imposes an additional excluded-volume constraint with other NPs: that is, the space between two bonded NP locations also cannot be occupied by other NPs. Physically, this assumption captures the fact that polymeric grafts must occupy the space between two merged patches and thus exclude all other NPs from occupying the same space. In a more general sense, even covalent bonding imposes a strong electron density inside the bonding orbitals between atoms that subsequently exclude other subatomic particles. Through this lens, adding effects of connectivity into EBT requires the inclusion of bonding directly in the construction of the shape orbitals for each respective particle geometry.

We first define an effective NP composed of a central core whose shape is commensurate with the NP geometry and spherical patches of size  $\sigma$  placed at NP surface locations exhibiting patch-patch merging interactions. The construction of this composite particle captures the physical picture that the patches themselves impose excluded volume constraints and thus directly influences the pP distribution. This approach generalizes **Eq. 1** to:

$$\beta U_m(r) = \beta U_{pP}(r) + \sum_{i}^{N} \beta U_{core}(r) + \sum_{i}^{M} \left[ \beta U_{patch}(r_p) + \beta U_{pP}(r_p) \right]$$
(3)

where M indicates the total number of patches,  $U_{patch}(r)$  define the hard-core repulsion between pPs and spherical patches of size  $\sigma$ , and  $\beta U_{pP}(r) \equiv r^{-2} \left[ \ln \rho_{pP}(r) - \beta \mu_{pP} \right]$  (for ease of notation). The first two terms in **Eq. 3** account for the effect of the NP core on the pP distribution and carry over from EBT. The last two terms extend EBT to consider the effect of the patches on the resulting

pP distribution. Note that the  $r_p$  coordinate indicates a relative distance to the patch locations with respect to the NP frame of reference. To account for patch-patch connectivity, we further extend Eq. 3 to sum over all pairwise bonding between patches, yielding:

$$\beta U_{m}(r) = \beta U_{pP}(r) + \sum_{i}^{N} \beta U_{core}(r) + \sum_{i}^{M} \left[ \beta U_{patch}(r_{p}) + \beta U_{pP}(r_{p}) \right] + \sum_{m} \beta U_{harmonic}(r_{b})$$

$$(4)$$

$$U_{harmonic}(r_b) = k_h(r_b - r_o)^2 \tag{5}$$

where the final summation is over the set of m pairwise bonds within the system,  $r_o$  is the bond length arising between the merged patches,  $r_b$  defines relative coordinate system between the pP and the two bonded patches, and  $k_h$  is the spring constant associated with the bond potential. For our derivations, we assume a simple harmonic potential for  $U_{harmonic}$  between merged patches (Eq. 5). By inspection, the first two terms in Eq. 4 only applies to the NP core and the last three terms only operate on the patches. Since the patches and core are independent particles within the effective NP, Eq. 4 suggests that the effective shape orbital for each patchy NP can be constructed via a superpositioning of individual pP distributions. In other words, the cEBT generalization defines the total  $\rho_{pP}$  as a composite pP density distribution that arises from adding together a pP distribution for only the core NP ( $\rho_{core}$ ) and a pP distribution for patches decorating the NP surface  $(\rho_{vatch})$ : that is,  $\rho_{pP} = \rho_{core} + \rho_{vatch}$  (**Appendix A**). This is analogous to constructing molecular orbitals via a linear combination of atomic orbitals (LCAO) commonly employed in QM calculations for molecules<sup>40,41</sup>. Fig. 1e shows the shape orbital obtained from cEBT for a single triangle and cube where connectivity locations are placed at the vertex of the shape, respectively. Similar to EBT, Eqs. 4 - 5 is for the limit of a single reference patchy NP. Generalization to multiple patchy NPs is a straightforward summation over individual  $\rho_{pP}$  corresponding to each NP within the system. Solving Eq. 4 for pairs of bonded triangles (Fig. 1f,g) and cubes (Fig. 1h,i) reveal the effect of connectivity on stable configurations between NPs, where the same relative NP orientation but with an overstretched bond produces a significantly higher net total free energy (less stable configuration) between particles (Fig. 1j). Furthermore, plotting the predicted bonding potential as a function of NP center-to-center separation (Fig. 1k) reveals a nearly identical functional form to the finitely extensible nonlinear elastic (FENE) potential commonly used for flexible polymers<sup>42</sup>. These results indicate that cEBT can reproduce the flexible bonding that naturally arises from patch-patch merging between interacting NPs observed in experiments<sup>33</sup>.

Equilibrium Chain Conformation for Polymeric NPs. Results from pairwise calculations between bonded NPs immediately suggest that oligomers/polymers of connected NPs will also experience significant orientational constraints with respect to their equilibrium inter-NP orderings. Motivated by the polymer-like bonding potential between NPs (Fig. 1k), we borrow ideas from polymer physics to develop an analytical theory aimed at predicting the conformational behaviors for long chains of connected patchy NPs. Specifically, it is well known that the equilibrium scaling behavior for chain size (R) is  $R \sim N^{1/2}b$ , where N is the degree of polymerization and b is the size of the Kuhn monomer<sup>43</sup>. This classical behavior, however, assumes that monomers are spherical and cannot capture shape-driven orientational orderings that dominate in the limit of anisotropic geometries<sup>44–46</sup>. To account for the effects of anisotropy in dictating chain conformation, we first note that the  $R \sim N^{1/2}$  scaling relationship is obtained via a random-walk derivation. Here, we introduce a variant of a biased random walk model where a step left is different in size than a step right: that is,  $b_{left} \neq b_{right}$ . This model reflects the idea that different modes of bonding (i.e. vertex-vertex, edge-edge, or face-face) can result in uneven forward/backward steps due to geometric constraints imposed by the underlying particle shapes. Performing a statistical mechanical derivation of the equilibrium chain size for a 3D polymer composed of anisotropic monomers yields (Appendix B):

$$R \sim N^{(2-\Lambda)/2} b_P \tag{6}$$

where  $\Lambda$  is a value between 0 and 1 that accounts for different bonding locations and bond lengths between monomers, and  $b_P$  defines the size of each NP monomer. Specifically,  $\Lambda=0$  corresponds to a bond that connects a monomer's largest facet to the same facet on a neighboring monomer (face-face connected patches on a cube). Conversely,  $\Lambda=1$  corresponds to vertex-vertex bonding between monomers. Eq. 6 assumes that all the monomers have the same inter-monomer connectivity. In the limit of a spherical monomer,  $\Lambda=1$  as all surface bonding locations exhibit the same energy. By inspection, Eq. 6 reproduces the well-known gaussian chain statistics for a spherical monomer  $R \sim N^{1/2}b_P$ . However, for anisotropic monomers where  $\Lambda$  is not uniformly 1, we immediately see that chains can exhibit a diverse suite of conformations that depends on bonding locations between monomers. Furthermore, we note that Eq. 6 is agnostic of length-scale.

This means that its predictions readily apply to nano/colloidal polymers composed of connected, anisotropic NPs/colloids as well as for traditional polymers containing monomers with more complex geometries such as conjugated/aromatic moieties or molecular polyhedra (POSS, carborane, and/or fullerenes).

## **Experimental Validation of cEBT and Anisotropic Polymer Scaling**

**cEBT for Patchy Triangular Nanoprisms.** Results from the experimental literature have shown that vertex-vertex connected triangular NPs mediated by patch-patch merging produce an equilibrium motif where edges are slanted towards each other (saw-tooth) as opposed to the expected tip-to-tip configuration (bowtie)<sup>33</sup>. Furthermore, the emergent inter-NP bonding arising from patch-patch merging are reported to be highly flexible and can freely rotate in solution<sup>33</sup>. Here, we employ cEBT (Eqs. 3-5) to provide a microscopic picture of the underlying driving force governing both the formation of the saw-tooth motif as well as the observed emergent bond flexibility. Fig. 2f shows a free energy surface for vertex-vertex connected NPs as a function of relative NP orientations for a patch size  $\sigma$  equal to 25% of the NP edge length ( $s_{NP}$ ): that is, 0.25  $S_{NP}$ . This patch size is commensurate to the experimentally measured polymeric patches that form on triangular NPs<sup>33</sup>. Results from cEBT calculations indicate that the lowest energy configuration between connected NPs is the saw-tooth motif, in agreement with experimental findings (Fig. 2f). The equilibrium configurations are plotted as inset in each of their respective free energy surface in Fig. 2 and their locations on each free energy surface are indicated by red stars. Inspection of the bonding orbitals between NPs clearly indicates that the saw-tooth configuration provides a higher overlap between shape orbitals located at the triangular edges. These edge-localized orbitals are entropic in nature since they arise due to particle geometry and not from patch-patch bonding interactions (Fig. 1). Therefore, the saw-tooth motif is unique to nanoscale patchy NPs and arise due to a direct competition of two counteracting forces: 1). directional entropic forces favoring edge-edge alignment and 2). patch-patch merging favoring vertex-vertex alignment. It is this delicate balance between opposing forces that breaks the symmetry intrinsic to the preprogrammed vertex-vertex patchy interactions.

Furthermore, the computed energy difference between different relative NP configurations is on the order of  $1 \, kT$  (Fig. 2f). This means that the bonds between NPs are not orientationally locked but can transition between one state versus another since their energetic differences are on the order of thermal noise. As such, cEBT predicts that the emergent inter-NP bonding resulting

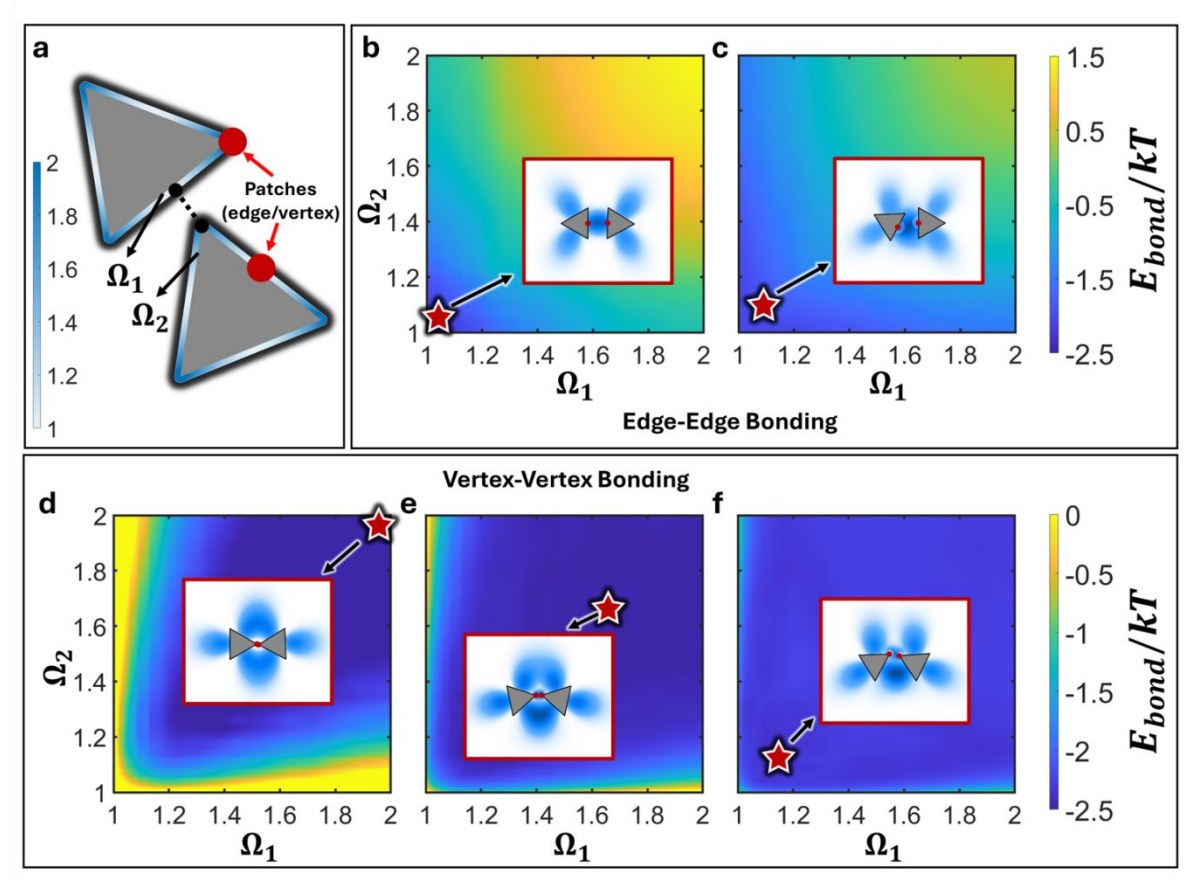


**Figure 2. cEBT Energy Surface for 2D Triangle.** a) Definition of shape factor  $\Omega$  to indicate surface site on triangle. Relative orientations between two triangles are indicated by the closest point of contact on the surface of each respective triangle ( $\Omega_1$  and  $\Omega_2$ ). Red points indicate the patch location. Free energy surface for edge-edge connected triangles with patch size b) 0.1  $s_{NP}$  and c)  $0.3s_{NP}$ . Bonding energy indicates that edge-edge alignments become disfavors with larger patch sizes. Free energy surface for vertex-vertex connected triangles with patch size d)  $0.05s_{NP}$ , e).  $0.15s_{NP}$ , and  $0.25s_{NP}$ . Results show a shift from bowtie to sawtooth as the lowest energy structure with increasing patch sizes. Insets plot the lowest energy configuration between the bonded triangles and red stars indicate the location of the stable configuration on the free energy landscape.

from patch-patch merging is highly flexible, which is also congruent with experimental observations<sup>33</sup>. Combined, cEBT calculations provide a microscopic understanding of the underlying forces at play that govern both the emergent bond flexibility between NPs as well as their equilibrium saw-tooth configurations.

The critical balance between entropy versus enthalpy in directing orientational ordering between NPs sits in direct contrast to traditional patchy colloids that have been reported in the literature<sup>13,28,30–32,35</sup>. In patchy colloids, patch-patch interactions are inflexible and uniquely define the directional interactions between particles: that is, a vertex patchy colloid can only produce

vertex-vertex assembly configurations. This is because patches for colloidal particles are small relative to the core size compared to their NP counterparts. As a result, patch-patch bonding in the colloidal limit experience high steric hinderances. Since cEBT is agnostic of scales, decreasing the patch size in our calculations should also capture the behaviors of patchy colloids. Indeed, reduction of the patch size to  $0.15s_{NP}$  shifts the equilibrium structure to the bowtie configuration (Fig. 2e). However, since the patch sizes are still roughly on par with the core size, the difference in energy between bowtie and saw-tooth configurations are still within thermal noise (Fig. 2e). Decreasing patch size further to  $0.05s_{NP}$  show a marked shift in the free energy surface, where the bowtie configuration is now highly energetically favored with energy differences on the order of 3 kT (Fig. 2d). In other words, transitions between the bowtie and sawtooth configurations are no longer favorable at this small patch size. This behavior converges cEBT calculations to the limit of patchy colloids where particle sizes are much bigger than patch sizes, indicating that cEBT can accurately model patchy interactions across multiple length scales.

Since entropy-driven interactions favor edge-edge alignments between the triangular NPs, it is natural to expect that patch-mediated edge-edge connected NPs will favor only edge-edge alignments. Indeed, cEBT energy calculations at patch sizes equal to  $0.1s_{NP}$  reveal that only edgealigned NPs are favored (Fig. 2b). Furthermore, the total free energy between the equilibrium configurations is lower than those observed for vertex-vertex bonded NPs, indicating that entropic effects complement patch-patch connectivity in such edge-aligned cases. However, increasing patch size to  $0.3s_{NP}$  shows a shift away from edge-edge alignments between particles (Fig. 2c). Inspection of the bonding orbitals obtained from cEBT indicates that excluded volume interactions between larger patch sizes push NPs so far apart that a tilted state produces higher shape orbital overlaps relative to the edge-aligned configuration. These equilibrium configurations are shown in the inset for each free energy surface in Figs. 2b,c. In addition to triangular NPs, we computed the potential energy surfaces for several other vertex-vertex connected 2D geometries (Appendix **D**) including square (SI, Fig. D1a), pentagonal (SI, Fig. D1a), and hexagonal (SI, Fig. D1a) NPs. Analysis of the equilibrium configurations for patch sizes commensurate with particle edge lengths all reveal that directional entropic forces systematically break tip-to-tip alignments between NPs to favor tilted configurations between NPs at large patch sizes.

**cEBT and Scaling Prediction of Peptide Bundlemers.** To further showcase the generalizability of cEBT and the developed anisotropic chain scaling theory, we apply our calculations to

covalently bonded coiled-coil bundles (bundlemers) previously reported in the literature<sup>38</sup>. Briefly, each bundlemer is a nanoscale unit constructed from 4  $\alpha$ -helical peptide oligomers that fold into well-defined, anti-parallel coiled-coil bundles roughly 4 nm in length and 2.5 nm in diameter. Each individual  $\alpha$ -helix tail contains a maleimide or thiol group that can undergo a thiol-Michael reaction to form covalent bonds between neighboring bundlemers that are typically 0.2 nm in length. Based on the folded coiled-coil geometry, there are two covalent bonding sites at the top and two at the bottom of the long axis for each bundlemer (**Fig. 3a**). In essence, the effective geometry for this nanoscale building block is that of a cylinder with height h and two patchy sites of size 0.05h: one at the top cylinder face and one at the bottom cylinder face (**Fig. 3a**, top). Performing cEBT and scaling exponent calculations for these bundlemers reveal a linear, rod-like behavior with v = 0.97 (**Fig. 3a**), in excellent agreement with experimentally observed formation of long, rigid rods.

Furthermore, experiments reported the formation of more flexible bundlemer chains upon transitioning to a PETMP thiol linker between bundlemers. This new PETMP linker corresponds to a new patch size of 0.15h between each NP (Fig. 3b, top). Predictions using the increased bond length in cEBT reveal a shift the equilibrium pairwise configuration to a tilted alignment between cylinders (Fig. 3b), which corresponded to a new scaling exponent of v = 0.88. Combined, these results indicate that increasing bond flexibility shifts chain conformation from that of a rigid rod to a semiflexible chain, which matches experimental observations. Lastly, experiments also enabled a lateral bonding mode between bundlemers mediated via 2 nm gold NPs functionalized with maleimide (Fig. 3c, top). This new lateral bonding mode results in a mix between lateral and face-face aligned bundlemers in experiments (Fig. 3c). Within our cEBT model, the new NP linker corresponds to a 0.5h patch size located at the rim of the cylinder. Performing calculations for this new patchy motif and visualizing the lowest energy configuration reveal similar relative orientations between bundlemers compared to those observed in experiments (Fig. 3c). More specifically, cEBT calculations indicate that the energy differences are on the order of 0.1kT, indicating that both motifs are thermodynamically favorable, providing a microscopic understanding of the emergent bonding behaviors. We additionally predict that the scaling exponents drops to v = 0.75. This means that chains formed via lateral bonding between

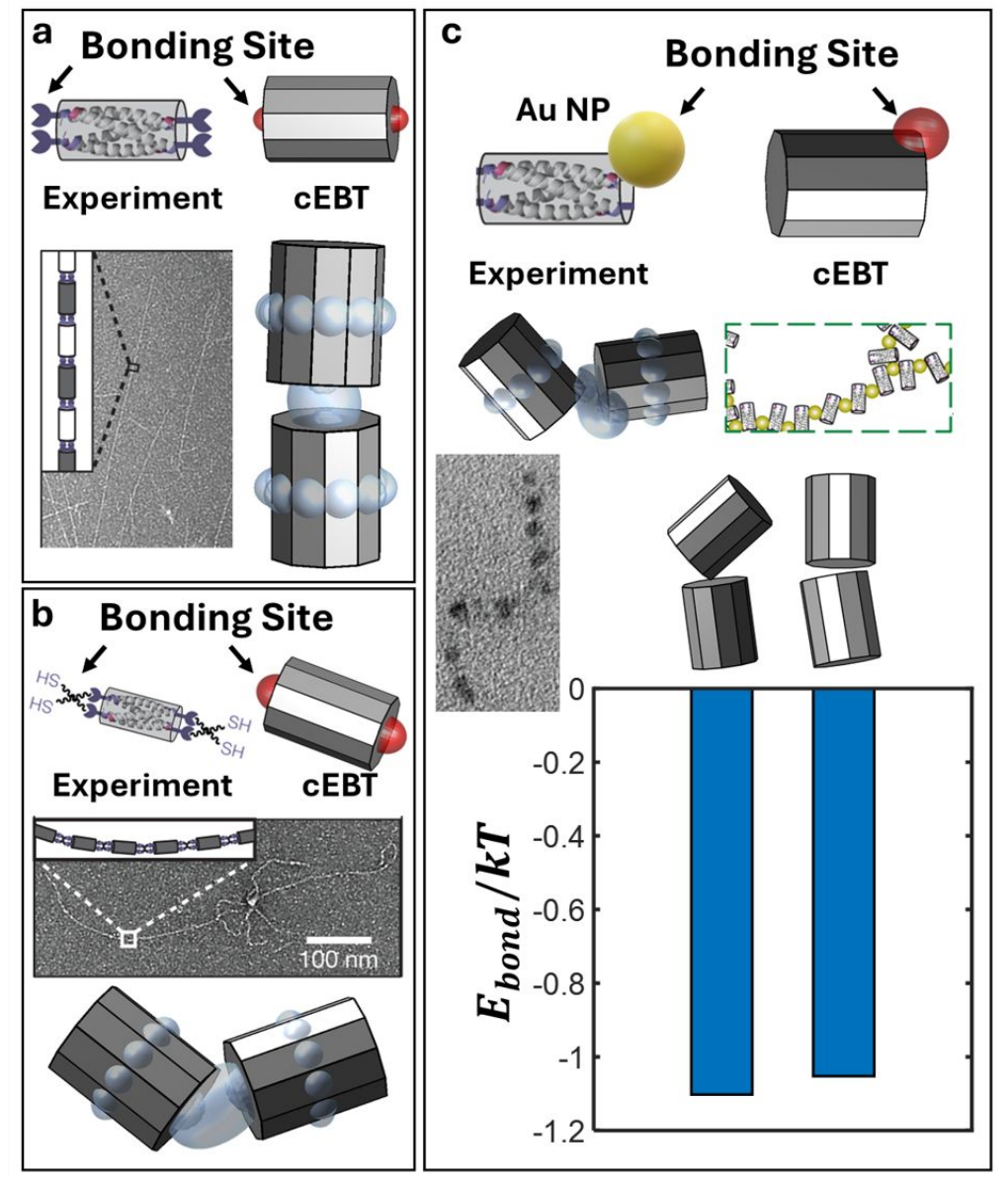


**Figure 3. cEBT Prediction of Polymeric Bundlemers.** Equilibrium configuration predicted using cEBT sampling across all relative orientations between bundlemers (modelled as cylinders) for a) face-face connection using rigid linkers, b) face-face connection using flexible linkers, and c) edge-edge connection. For each panel, the top indicates how the experimental system is mapped to the cEBT model. All predicted cEBT prediction matches with the experimentally observed bonding motif between bundlemers. In the limit of edge-edge connection, the relative free energy different between tilted and face-face alignment is shown to be on the order of  $\sim 0.1kT$ , corroborating the mixed motif observed in experiments. All experimental images are reproduced with permission<sup>38</sup>.

bundlemers are much more flexible compared to their face-face bonded counterparts, in agreement with the experimentally reported chain conformations being more flexible and random relative to the above two cases. Not only do these findings provide additional validations of cEBT, but they

also emphasize the universality of our theories by showing that both cEBT (**Eqs. 3** – **5**) and anisotropic chain scaling (**Eq. 6**) applies to both inorganic NP monomers as well as biological, peptide-based polyhedral monomers.

#### **Simulation Methods**

While comparison with established literature provide validation testbeds for specific limits of cEBT and anisotropic scaling predictions, we further seek to showcase the broad generalizability of our developed theory to arbitrary monomer geometry as well as bonding modes. Along this vein, we perform simulations for polymer chains consisting of anisotropic monomeric units using the HOOMD-Blue package<sup>47</sup>. Specifically, we consider two different types of bonding potentials – harmonic and FENE. These potentials are selected due to their usage across a wide range of coarse-grained polymer simulations. For example, the FENE potential is the model of choice for traditional bead-spring polymer simulation and has recently been shown to accurately capture the dynamics of bonded patchy NPs observed in simulations<sup>33</sup>. Common force fields such as CHARMM<sup>48</sup>, AMBER<sup>49</sup>, and MARTINI<sup>50,51</sup> readily fit parameters to the harmonic potential to capture the behaviors of traditional polymers such as those containing conjugated and/or charged moieties. As such, validating predictions across these common coarse-grained models will ensure that our theory can be readily applied to a diverse range of both nano/colloidal as well as traditional polymeric systems.

Anisotropic Polymers Bonded via the FENE Potential. We employ molecular dynamics (MD) to characterize the equilibrium scaling behavior of polymeric chains made of anisotropic building blocks bonded via the FENE potential. Each system is set up on HOOMD-Blue as a single chain of bonded anisotropic particles immersed in an implicit-solvent with chain lengths varying from 40 to 200. Simulations are carried out using an NVT ensemble at a temperature of kT = 0.9 and employ the Nosé-Hoover thermostat and the MTK equations<sup>52,53</sup>. We perform simulations for both spherical monomers as well as three different monomer geometries: cube, octahedron, and tetrahedron. Anisotropic particles are bonded together edge-edge, face-face, or vertex-vertex using patches that are rigidly attached to the core particle at each respective bonding location (**Fig. 4**). Bonds between patches use the FENE potential:  $\beta V(r) = -0.5kr_0^2 \ln\left(1-\left(r/r_o\right)^2\right) + V_{WCA}(r)$  where  $V_{WCA}(r)$  is the Weeks-Chandler-Andersen repulsive interaction<sup>54</sup>. The parameters employed in simulations are k = 30 and  $r_o = 1.5a$ , with a = 10. The core monomers are treated as repulsive hard-particles using the anisotropic Lennard-Jones potential<sup>55</sup>. A typical FENE bond

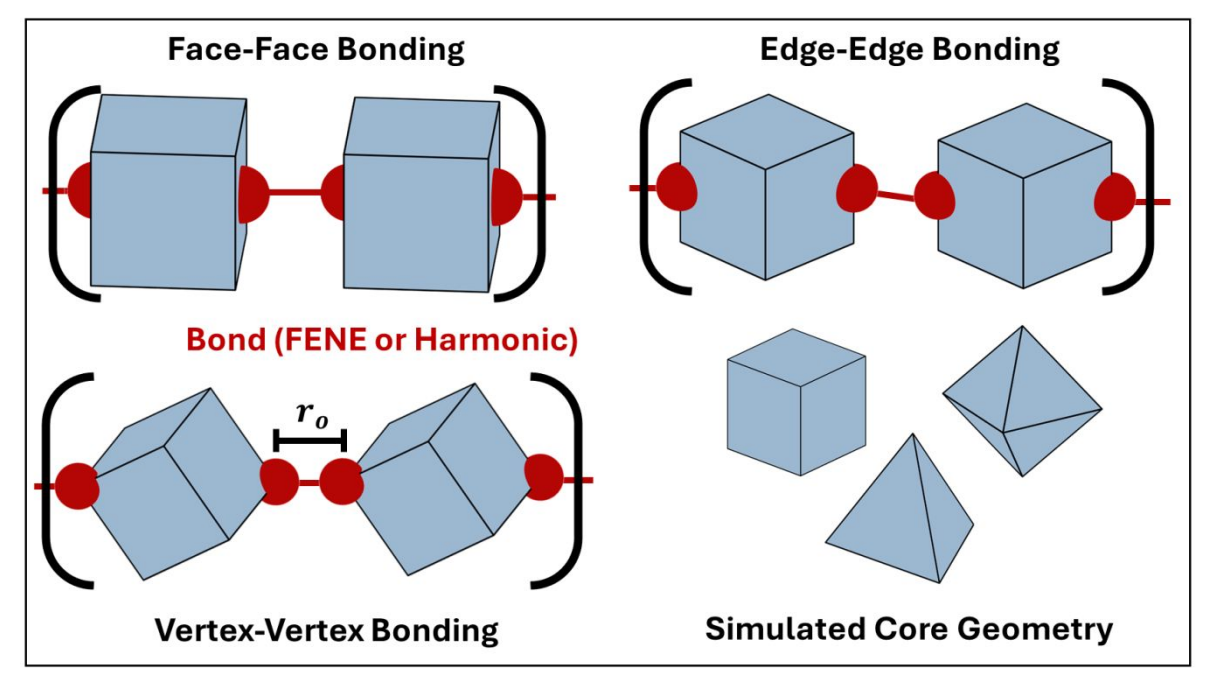


**Figure 4. Computational Model for Anisotropic Polymers.** Schematic of simulated polymers constructed from anisotropic monomeric units: cube, octahedron, and tetrahedron. Bonds are explicitly constructed at the desired location bonding location (vertex-vertex, faceface or edge-edge). Simulations are performed using both the harmonic and FENE potentials.  $r_o$  indicates the bond length and N represents the degree of polymerization.

has an equilibrium bond length of 0.89a. This translates to effective patch sizes of 10% of the insphere diameter  $(\sigma_{in})$  of the cube and octahedron, and 20% of the insphere diameter  $(\sigma_{in})$  of the tetrahedron. The step-size is  $dt = 5 \times 10^{-4}$  for octahedra and cubes, and  $2.5 \times 10^{-4}$  for tetrahedra. All systems are run for 25,000 simulation time units.

Anisotropic Polymers Bonded via Harmonic Potential. We perform Monte Carlo simulations for four different types of particles – patchy spheres, tetrahedron, cube, and octahedron – bonded using the harmonic potential. For each shape, two different modes of bonding are performed: vertex-vertex and face-face. For vertex-vertex bonding, connection sites are placed along the polyhedron's diagonal (**Fig. 4**). For face-face bonding, connection sites are positioned at the center of opposing faces for each respective shape (**Fig. 4**). The bonding potential employed for the Metropolis algorithm<sup>56</sup> is:

$$\beta V_{bond} = \sum_{s}^{N-1} \frac{3}{2r_o^2} b_s^2 \tag{7}$$

where N is the chain length and  $b_s$  is the  $s^{th}$  bond length.  $r_o$  is the equilibrium bond length and is identical to the patch size from cEBT calculations. Larger values of  $r_o$  correspond to larger bond

Table 1. Connection Between Polymer Simulation and cEBT			
Patch Size	Simulation	cEBT	
Small (S)	$r_o = 0.1\sigma_{in}$	$\sigma = 0.1\sigma_{in}$	
Medium (M)	$r_o = 0.5\sigma_{in}$	$\sigma = 0.5\sigma_{in}$	
Lorgo (L)	$x = F \Omega \sigma$	$\sigma = E \Omega \sigma$	

 $r_o$ : equilibrium bond length,  $\sigma_{in}$ : monomer insphere diameter,  $\sigma$ : patch size. **FE**: FENE bonding, **HR**: Harmonic bonding

lengths (patch sizes) between particles and more flexible bonds. For our simulations, we consider three different  $r_o$  values of 0.1, 1, and 5, which correspond to 10%, 100%, and 500% of the insphere diameter ( $\sigma_{in}$ ) for each respective monomer geometry. All other interactions between particles are set to be sterically repulsive. Simulations are performed for chains lengths ranging from 10 to 80. Maximum displacement and rotational trial moves are set equal to the equilibrium bond length ( $r_o$ ) and 0.5, respectively. The ratio between rotation and translation trial is equal to 0.5. Each particle is selected four times to perform movements per HOOMD-Blue integration step. All simulations are run for approximately 1E7 Monte Carlo moves. Larger systems are run for up to 7E7 Monte Carlo moves for better statistics.

### Computational Validation of cEBT and Anisotropic Polymer Scaling

Connections Between FENE and Harmonic Potential Simulation and cEBT. For clarity, we note that simulations using the FENE potential have effectively identical patch sizes to those for harmonic potential with  $r_o = 0.1\sigma_{in}$ , where  $\sigma_{in}$  is the anisotropic particle's insphere diameter. We define this as the "small patch" limit to connect to theoretical cEBT and scaling calculations for the same patch size of  $\sigma = 0.1\sigma_{in}$ . Similarly, harmonic potential simulations with  $r_o = 0.5\sigma_{in}$  are defined as the "medium patch" limit to enable a direct comparison with theory calculations for patch size of  $\sigma = 0.5\sigma_{in}$ . Lastly, the "large patch" limit refers to harmonic potential simulations with  $r_o = 5.0\sigma_{in}$ , which corresponds to theory calculations for patch size of  $\sigma = 5.0\sigma_{in}$ . For ease of notation, we use FE and HR to indicate FENE and harmonic bonding, respectively. These connections are summarized in **Table 1**. Scaling exponents showing that our patchy bonding models reproduces known behaviors for traditional polymers with spherical subunits are reported in **Appendix C** of the SI.

Equilibrium Configurations and Chain Scaling for Cubic Monomer Geometry. We first discuss results for cubic monomer geometry. Here, we employ cEBT (Eqs. 3-5) to compute the free energy between vertex-vertex and face-face connected cubes. Across all bonding modes,

analysis of the lowest energy configuration reveals the formation of symmetry breaking orientational ordering between NPs. Similar to their 2D counterparts (**Fig. 2**), visualization of the bonding orbitals of the equilibrium NP configurations reveals that maximization of shape orbital overlaps serves as the dominant driving force underpinning the observed symmetry breakage in NP relative orientation (**Fig. 5a,f**).

Starting with face-face bonded cubes, we employ cEBT (Eqs. 3 - 5) to compute the bonding free energy  $(E_{bond})$  for all pairwise relative orientations between cubes indicated in Fig. 5b. This large sweep ensures that we have properly sampled all possible orientations between cubes. Due to the high dimensionality of this phase space, we chose to compare the computed  $E_{bond}$  between the two identified lowest energy configurations (face-face and face-edge) for small medium patches mediating face-face connections. Specifically, we plot the computed  $E_{hand}$  for face-face and face-edge configurations in the limit of small patches (left, Fig. 5a) and the same two configuration energy but in the limit of medium patches (right, Fig. 5a). Colors for each energy plot correspond to the color of the boxed relative orientations in Fig. 5a. Results indicate that faceface aligned cubes are only favored in for small patches where the short bond length restricts bond flexibility, thereby preventing the system from rotating to seek additional shape orbital overlaps. Indeed,  $E_{bond}$  computed for face-edge oriented cubes in the limit of small patches shows that the total free energy is significantly higher compared to that of face-face alignment, indicating that it is less thermodynamically favored. Consequently, shifting to medium patches enhances bond flexibility and thus  $E_{bond}$  for face-face aligned cubes is now higher compared to face-edge aligned cubes due to additional overlaps between shape orbitals protruding from the cubes' other faces.

To compare simulations to cEBT pairwise calculations, we first compute the set of closest surface points between bonded monomers along the polymer backbone from simulations and plot their distribution on the surface of a reference monomer shape. **Fig. 5c** (top) shows the computed closest surface point distribution from simulations for face-face bonded cubes in the limit of small patches. Results indicate that the face-face alignment is the most dominant motif across all monomer-monomer relative orientations. These findings are in excellent agreement with pairwise cEBT energy calculations for small patches (**Fig. 5a**), where face-face aligned configurations are thermodynamically favored. To bridge pairwise calculations to the polymer limit, we measure the

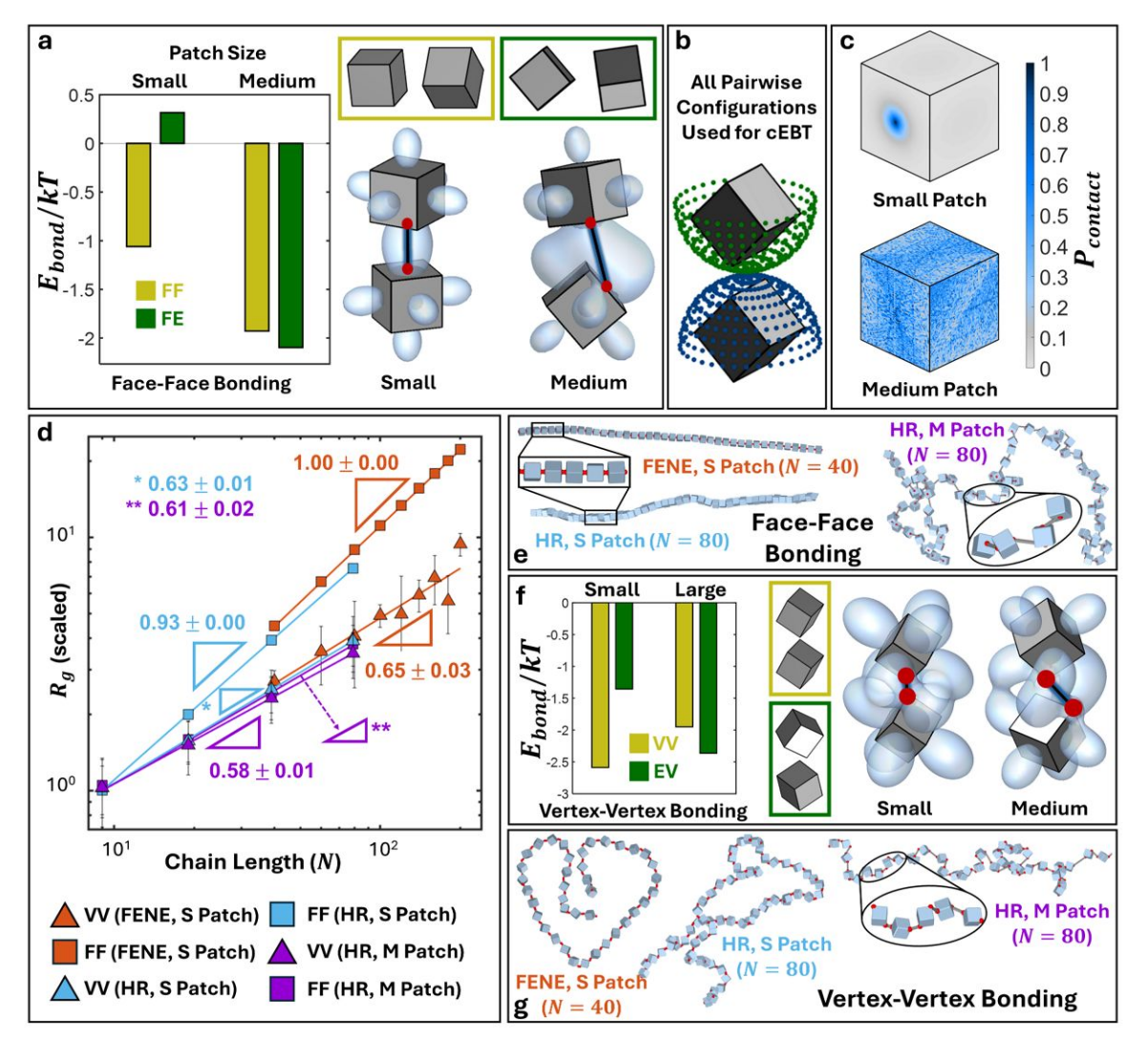


**Figure 5. Polymers with Cubic Monomeric Subunits.** a) cEBT for small versus medium patches for face-face bonded cubic NPs. Yellow box shows the lowest energy configuration for small patches (face-face) and green box shows the lowest energy configuration for medium patches (face-edge). Plotted  $E_{bond}$  compares the energy of the predicted equilibrium configurations for small and medium patches. Bonding configuration and orbitals are visualized for the lowest energy configuration each respective patch size. b) Set of all pairwise relative orientations utilized in cEBT calculations. c) Closest surface contact point distributions ( $P_{contact}$ ) for face-face bonded cube with small (top) and medium patch sizes (bottom). d)  $R_g$  vs N scaling fits for face-face and vertex-vertex bonded polymeric chain of cubes for small and medium patch sizes across both FENE and harmonic (HR) bonding potential simulations. e) Simulation snapshots for face-face bonded cubes for small and medium patch sizes. f) Similar cEBT analysis to panel a) for vertex-vertex bonded cubes. g) Simulation snapshots for vertex-vertex bonded cubes for small and medium patch sizes. Abbreviation definition: face-face (FF), vertex-vertex (VV), face-edge (FE), edge-vertex (EV).

end-to-end scaling exponent v ( $R_g \sim N^v$ ) for polymer chains constructed from face-face bonded

cubic monomers from simulations. **Fig. 5d** shows an  $R_g$  vs N scaling exponent plot for simulation results using both harmonic and FENE bond potentials for cubic systems. For face-face bonding, small patches yield a scaling exponent of  $v = 1.00 \pm 0.00$  and  $v = 0.93 \pm 0.00$  for the FENE and harmonic potentials, respectively. These values suggest that chains are extended and experience a high degree of orientational constraints between neighbors. Indeed, theory prediction of the scaling exponent for face-face bonded cubes in the limit of small patches (**Eq. 6**) gives v = 1, in agreement with simulations. Physically, a scaling exponent of v = 1 indicates that chains exhibit rigid, rod-like behaviors. Visualizations of chain conformation in this limit additionally confirm this interpretation as we only observe straight chains of face-face aligned cube across both FENE and harmonic potential simulations for small patch sizes (**Fig. 5e**).

Increasing to the medium patch size limit for cubes yields scaling exponents of  $v = 0.61 \pm 0.02$  from simulations (Fig. 5d), which closely matches the theoretically predicted value of v = 0.57. Similar to the small patch limit, we compare simulations to cEBT by computing closest surface points distribution between neighboring cubes and plotting the results on a reference particle (Fig. 5c, bottom). Results indicate a shift away from face-face aligned orientations to show a strong signature for face-edge alignments between neighboring monomers, in exact agreement with theory calculations from cEBT (Fig. 5a). Through the lens of increased rotational freedom between neighboring cubes, monomers effectively behave akin to overlapping spherical monomers whose radii are equal to the shape's midsphere radii. This means that connected cubes partially feel the effect of sterically-driven excluded volume interactions for all relative orientations where the shape sits outside the volume occupied by its midsphere. By definition, this is a self-avoiding walk and thus the chain scaling matches the classically known exponent of v = 0.6 for such systems. Visualization of chain conformation for face-face connected cubes in the limit of medium patch sizes further confirms the predictions from theory, where chains exhibit worm-like features intrinsic to self-avoiding conformations (Fig. 5e). Lastly, shifting further to the large patch size limit results in a scaling exponent of  $v = 0.5 \pm 0.003$  for face-face bonded cubes (Appendix I), which is congruent with theory prediction for v = 0.5. In this limit, the large patch size forces monomers so far apart that they do not feel the presence of their neighbors, enabling an unrestricted degree of rotational freedom between bonded cubes. In other words, particles lose knowledge of both their core geometry as well as bonding constraints with their neighbors and behave akin to highly overlapping spherical monomers. This is analogous to a

traditional random walk and thus the scaling exponents converge to the well-known gaussian scaling statistics<sup>43</sup>.

Fig. 5f shows an analogous analysis of cEBT pairwise calculations for vertex-vertex bonding between cubes, where we observe an orbital overlap driven shift from a vertex-vertex to an edge-vertex motif with a corresponding increase from small to medium patch size. Unlike faceface bonding, the measured scaling exponents for both small and medium patch sizes yield similar values of  $v \sim 0.6$  (Fig. 5d), indicating that chains behave akin to self-avoiding walks between neighboring monomers. This difference relative to their face-face bonded counterparts arises due to the bonding location between neighboring cubes. If we trace the vertex of a cube spinning about its center of mass, the effective geometry that the vertex sweeps out is a sphere whose diameter is equal to the cube's circumsphere. As a result, each cube perceives its neighbor not as a cube but rather as a sphere whose effective diameter is equal to the circumsphere diameter of its neighboring cube. However, since the cubes take up less space than their circumsphere, the neighboring circumspheres are not orientationally locked into a linear, vertex-vertex aligned motif, but can partially overlap with each other. This behavior is also akin to a self-avoiding walk, which is known to exhibit scaling exponent of v = 0.6. Visualization of the equilibrium chain conformation for vertex-vertex bonded cubes for both small and medium patch sizes all reveal worm-like chain conformations, further corroborating the predicted self-avoiding walk scaling statistics (Fig. 5g). Similar to face-face bonding, the large patch limit for vertex-vertex bonding yields the trivial gaussian limit where monomer lose knowledge of both their geometry and bonding constraints. Analogous results are also obtained for edge-edge bonding between cubes and are reported in **Table I1** and **Appendix H** of the SI.

Polymeric Chains with Octahedral and Tetrahedral Monomer Geometries. Additionally, we perform the same cEBT calculation for octahedra (SI, Fig. E1b,c) and tetrahedra (SI, Fig. E1d,e) for all connectivity – face-face, edge-edge, and vertex-vertex (Appendix E). Across all shapes and connectivity, the consistent cEBT prediction is that connectivity only locks particle configurations in the limit of small patches. Medium patches allow for higher bond flexibility, resulting in a complex interplay between connectivity constraints and directional entropic interactions to give rise to symmetry breaking orientations such as edge-vertex, face-edge, and face-vertex motifs. Similar to cubes, we compare cEBT pairwise calculations with the closest surface point distribution between bonded monomers measured from simulations. Fig. 6c shows the computed

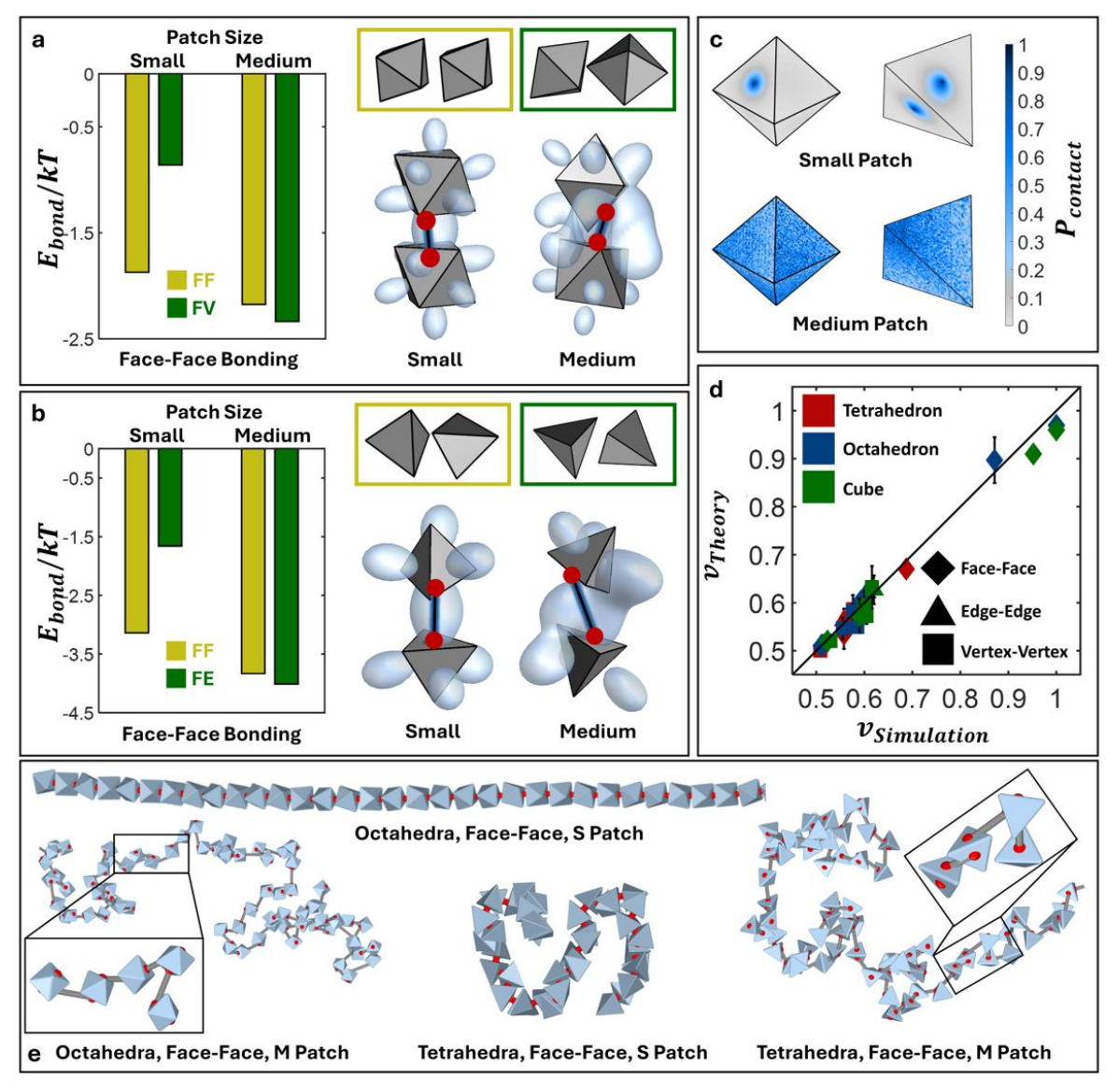


Figure 6. Polymers with Octahedral and Tetrahedral Monomeric Subunits. cEBT for small versus medium patches for face-face bonded a) octahedral NPs and b) tetrahedral NPs. Yellow box shows the lowest energy configuration for small patches and green box shows the lowest energy configuration for medium patches. c) Closest surface contact point distributions ( $P_{contact}$ ) for face-face bonded octahedra and tetrahedra with small (top) and medium patch sizes (bottom). d) Comparison of all scaling exponents for all shapes and all bond lengths between simulations versus theory. e) Simulation snapshots for polymers of face-face bonded octahedral and tetrahedral NPs for small and medium patches. Abbreviation definition: face-face (FF), face-edge (FE), face-vertex (FV).

distribution for face-face bonded octahedra and tetrahedra in the limit of small and medium patches. Octahedral monomers transition from face-face dominated to a face-vertex dominated distribution with increasing patch size. Similarly, tetrahedral monomers shift from a face-face dominated to a face-edge dominated motif. Both results are in agreement with cEBT predictions

for each respective monomer geometry (Fig. 6a,b). Visualization of the shift in chain conformation with increasing patch sizes are shown for both octahedral and tetrahedral monomers in Fig. 6e. Measured scaling exponents for such systems also progressively shift from rigid rod to selfavoiding walk to gaussian statistics as the patch size increases from small to medium to large, respectively. Analogous results are also obtained for vertex-vertex and edge-edge bonding between both octahedra and tetrahedra and are reported in **Appendix F**, **G**, and **I** of the SI. All the measured scaling exponents from simulations are accurately predicted using theory (Eq. 6). Fig. 6d encapsulates and compares all the scaling exponents from FENE and harmonic potential simulations against theory prediction, numerical values are tabulated in Table I1 of the SI. The tight agreement across theory and simulation indicates that the interplay between directional entropic forces and flexible patch-patch bonding between anisotropic monomers readily propagates to the oligomeric and polymeric scales and plays a critical role in controlling the equilibrium chain conformation. These findings highlight the success of our theory in illuminating the intricate balance between shape-driven and bond-driven interactions and how they work together to sculpt both local monomer-monomer ordering as well as global chain conformational statistics.

#### Conclusion

In summary, we elucidate how the interplay between patch-patch connectivity and shapedriven entropic interactions sculpts the spatial and orientational orderings between anisotropic building blocks. We show that emergent entropic forces can break the symmetry of the preprogrammed directional patchy (bonding) interactions between particles, especially in cases where patch sizes are more commensurate with NP core sizes. These results indicate that emergent entropic forces must be explicitly considered when designing patchy particles at the nanoscale as they can alter (or even break) the as-synthesized directional, patchy inter-NP interactions. Failure to consider such effects can produce situations where competing forces undermine the desired preprogrammed directional interactions and result in kinetically arrested and/or disordered assemblies. Our proposed cEBT development provides a theoretical framework for *a priori* prediction of this emergent symmetry breaking by explicitly accounting for both monomer geometry and connectivity constraints between particles. We validate cEBT by showing that it reproduces known behaviors from established experimental systems: patchy triangular nanoprisms and peptide bundlemers. Additionally, we rigorously validate cEBT against simulations for

polymer chains containing different particle geometries with different inter-NP bonding modes. Our analysis shows that cEBT not only captures the correct local ordering between NPs but also their macroscopic mesoscale ordering. In short, our work shines light on the complex forces at play with respect to patchy nanoscale building blocks with anisotropic geometries. The excellent agreement across theory, simulation, and validation against the experimental literature indicate that cEBT has the potential to expand the applicability of shape as a handle for directing self-assembly into the space of patchy NPs as well as molecular and colloidal polymers, opening newer doors for designing the self-assembly of novel soft, porous, and metamaterials.

#### Data Availability and Reproducibility Statement

Numerical data and results for structure and characterizations performed and shown in the main text are provided in the accompanying ZIP file with sample analysis scripts. Sample simulation scripts to perform both MC and MD simulations are included in the zip file. These analysis and simulation scripts will reproduce the data presented in all figures throughout the main text. We also provide sample simulation trajectory data (GSD file format) that represent the data/results that should come back from running the included files. All codes can also be found on our repository: https://github.com/VoGroupJHU/Anisotropic Chain.git.

#### Acknowledgements

This work is supported by start-up AFOSR Award Number FA9550-24-1-0100 and start-up funding provided by Johns Hopkins University. Simulation performed for this research used resources of the Advanced Research Computing Facility at Johns Hopkins University.

#### **Author Contributions**

K.A., X.Z., and T.V. designed and carried out the simulations. T.V. developed theory and directed the research. All authors contributed to the data analysis and writing of the manuscript.

#### **Competing Interests**

The authors declare no conflicts of interest.

#### **Materials and Correspondence**

Correspondence and materials requests should be addressed to Thi Vo at tvo12@jhu.edu.

#### References

- G. Chen, K. J. Gibson, D. Liu, H. C. Rees, J. H. Lee, W. Xia, R. Lin, H. L. Xin, O. Gang and Y. Weizmann, *Nature Materials*, 2018, **18**, 169–174.
- Y. Xiong, S. Yang, Y. Tian, A. Michelson, S. Xiang, H. Xin and O. Gang, *ACS Nano*, 2020, 14, 6823–6833.
- A. Kim, T. Vo, H. An, P. Banerjee, L. Yao, S. Zhou, C. Kim, D. J. Milliron, S. C. Glotzer and Q. Chen, *Nature Communications*, 2022, **13**, 1–14.
- 4 T. Vo, MRS Bull, 2024, 49, 330–339.
- 5 S. Ravaine and E. Duguet, *Curr Opin Colloid Interface Sci*, 2017, **30**, 45–53.
- 6 A. W. Long and A. L. Ferguson, *Mol Syst Des Eng*, 2018, **3**, 49–65.
- G. Doppelbauer, E. G. Noya, E. Bianchi and G. Kahl, *Soft Matter*, 2012, **8**, 7768–7772.
- 8 D. F. Tracey, E. G. Noya and J. P. K. Doye, *J Chem Phys*, 2019, **151**, 224506.
- 9 E. Bianchi, J. Largo, P. Tartaglia, E. Zaccarelli and F. Sciortino, *Phys Rev Lett*, 2006, **97**, 168301.
- 10 C. Karner, C. Dellago and E. Bianchi, *Soft Matter*, 2020, **16**, 2774–2785.
- 11 F. Romano, J. Russo, L. Kroc and P. Šulc, *Phys Rev Lett*, 2020, **125**, 118003.
- H. Liu, M. Matthies, J. Russo, L. Rovigatti, R. P. Narayanan, T. Diep, D. McKeen, O. Gang, N. Stephanopoulos, F. Sciortino, H. Yan, F. Romano and P. Šulc, *Science*, 2024, 384, 776–781.
- 13 Y. J. Kim, J. H. Kim, I. S. Jo, D. J. Pine, S. Sacanna and G. R. Yi, *J Am Chem Soc*, 2021, **143**, 13175–13183.
- Y. Tian, J. R. Lhermitte, L. Bai, T. Vo, H. L. Xin, H. Li, R. Li, M. Fukuto, K. G. Yager, J. S. Kahn, Y. Xiong, B. Minevich, S. K. Kumar and O. Gang, *Nature Materials*, 2020, 19, 789–796.
- W. D. Piñeros, M. Baldea and T. M. Truskett, *Journal of Chemical Physics*, 2016, **145**, 54901.
- B. A. Lindquist, R. B. Jadrich, W. D. Piñeros and T. M. Truskett, *Journal of Physical Chemistry B*, 2018, **122**, 5547–5556.
- 17 S. Lee, T. Vo and S. C. Glotzer, *Nature Chemistry*, 2023, **15**, 905–912.
- 18 T. C. Moore, J. A. Anderson and S. C. Glotzer, *Soft Matter*, 2021, **17**, 2840–2848.
- 19 T. Dwyer, T. C. Moore, J. A. Anderson and S. C. Glotzer, *Soft Matter*, 2023, **19**, 7011–7019.

- N. Pakalidou, J. Mu, A. J. Masters and C. Avendanõ, *Mol Syst Des Eng*, 2020, **5**, 376–384.
- 21 R. Guo, J. Mao, X. M. Xie and L. T. Yan, Scientific Reports, 2014, 4, 1–7.
- P. Kumar, T. Vo, M. Cha, A. Visheratina, J. Y. Kim, W. Xu, J. Schwartz, A. Simon, D. Katz, V. P. Nicu, E. Marino, W. J. Choi, M. Veksler, S. Chen, C. Murray, R. Hovden, S. Glotzer and N. A. Kotov, *Nature*, 2023, **615**, 418–424.
- D. Sahoo, M. R. Imam, M. Peterca, B. E. Partridge, D. A. Wilson, X. Zeng, G. Ungar, P. A. Heiney and V. Percec, *J Am Chem Soc*, 2018, **140**, 13478–13487.
- 24 M. A. Boles, M. Engel and D. V. Talapin, *Chem Rev*, 2016, **116**, 11220–11289.
- D. Samanta, W. Zhou, S. B. Ebrahimi, S. H. Petrosko and C. A. Mirkin, *Advanced Materials*, 2022, **34**, 2107875.
- 26 C. A. Mirkin and S. H. Petrosko, *ACS Nano*, 2023, **17**, 16291-16307.
- J. S. Kahn and O. Gang, *Angewandte Chemie International Edition*, 2022, **61**, e202105678.
- 28 É. Ducrot, M. He, G. R. Yi and D. J. Pine, *Nature Materials*, 2017, **16**, 652–657.
- 29 J. A. A. Diaz, J. S. Oh, G. R. Yi and D. J. Pine, *Proc Natl Acad Sci U S A*, 2020, 117, 10645–10653.
- 30 M. He, J. P. Gales, É. Ducrot, Z. Gong, G. R. Yi, S. Sacanna and D. J. Pine, *Nature*, 2020, **585**, 524–529.
- Y. Wang, Y. Wang, D. R. Breed, V. N. Manoharan, L. Feng, A. D. Hollingsworth, M. Weck and D. J. Pine, *Nature*, 2012, **491**, 51–55.
- T. Hueckel, G. M. Hocky and S. Sacanna, *Nature Reviews Materials*, 2021, **6**, 1053–1069.
- 33 A. Kim, K. Akkunuri, C. Qian, L. Yao, K. Sun, Z. Chen, T. Vo and Q. Chen, *ACS Nano*, 2024, **18**, 939–950.
- S. Stuij, J. Rouwhorst, H. J. Jonas, N. Ruffino, Z. Gong, S. Sacanna, P. G. Bolhuis and P. Schall, *Phys Rev Lett*, 2021, **127**, 108001.
- P. J. M. Swinkels, R. Sinaasappel, Z. Gong, S. Sacanna, W. V. Meyer, F. Sciortino and P. Schall, *Phys Rev Lett*, 2024, **132**, 78203.
- 36 W. Michaels, A. J. Spakowitz and J. Qin, *Macromolecules*, 2023, **56**, 8359–8368.
- 37 T. Vo and S. C. Glotzer, *Proc Natl Acad Sci U S A*, 2022, **119**, e2116414119.
- D. Wu, N. Sinha, J. Lee, B. P. Sutherland, N. I. Halaszynski, Y. Tian, J. Caplan, H. V. Zhang, J. G. Saven, C. J. Kloxin and D. J. Pochan, *Nature*, 2019, **574**, 658–662.
- 39 Z. Su, R. Zhang, X. Y. Yan, Q. Y. Guo, J. Huang, W. Shan, Y. Liu, T. Liu, M. Huang and S. Z. D. Cheng, *Prog Polym Sci*, 2020, **103**, 101230.

- P. Giannozzi, S. Baroni, N. Bonini, M. Calandra, R. Car, C. Cavazzoni, D. Ceresoli, G. L. Chiarotti, M. Cococcioni, I. Dabo, A. Dal Corso, S. De Gironcoli, S. Fabris, G. Fratesi, R. Gebauer, U. Gerstmann, C. Gougoussis, A. Kokalj, M. Lazzeri, L. Martin-Samos, N. Marzari, F. Mauri, R. Mazzarello, S. Paolini, A. Pasquarello, L. Paulatto, C. Sbraccia, S. Scandolo, G. Sclauzero, A. P. Seitsonen, A. Smogunov, P. Umari and R. M. Wentzcovitch, *Journal of Physics: Condensed Matter*, 2009, 21, 395502.
- 41 S. Lehtola, *Int J Quantum Chem*, 2019, **119**, e25968.
- 42 K. Kremer and G. S. Grest, *J Chem Phys*, 1998, **92**, 5057.
- 43 Z. G. Wang, *Macromolecules*, 2017, **50**, 9073–9114.
- 44 P. F. Damasceno, M. Engel and S. C. Glotzer, *Science*, 2012, **337**, 453–457.
- U. Agarwal and F. A. Escobedo, *Nature Materials*, 2011, **10**, 230–235.
- 46 S. Torquato and Y. Jiao, *Nature*, 2009, **460**, 876–879.
- 47 J. A. Anderson, J. Glaser and S. C. Glotzer, *Comput Mater Sci*, 2020, **173**, 109363.
- 48 S. Jo, T. Kim, V. G. Iyer and W. Im, *J Comput Chem*, 2008, **29**, 1859–1865.
- D. A. Case, T. E. Cheatham, T. Darden, H. Gohlke, R. Luo, K. M. Merz, A. Onufriev, C. Simmerling, B. Wang and R. J. Woods, *J Comput Chem*, 2005, **26**, 1668–1688.
- 50 S. J. Marrink, H. J. Risselada, S. Yefimov, D. P. Tieleman and A. H. De Vries, *Journal of Physical Chemistry B*, 2007, **111**, 7812–7824.
- P. Vainikka, S. Thallmair, P. C. T. Souza and S. J. Marrink, *ACS Sustain Chem Eng*, 2021, **9**, 17338–17350.
- 52 J. Cao and G. J. Martyna, *J Chem Phys*, 1996, **104**, 2028–2035.
- 53 G. J. Martyna, D. J. Tobias and M. L. Klein, *J Chem Phys*, 1994, **101**, 4177–4189.
- J. D. Weeks, D. Chandler and H. C. Andersen, *J Chem Phys*, 1971, **54**, 5237–5247.
- 55 V. Ramasubramani, T. Vo, J. A. Anderson and S. C. Glotzer, *J Chem Phys*, 2020, **153**, 084106.
- N. Metropolis, A. W. Rosenbluth, M. N. Rosenbluth, A. H. Teller and E. Teller, *J Chem Phys*, 1953, **21**, 1087–1092.

# Elucidating the Interplay Between Entropy-Driven and Patch-Mediated Bonding in Directing Nanoscale Assemblies

Kireeti Akkunuri<sup>1†</sup>, Xiangyu Zhang<sup>1†</sup>, Thi Vo<sup>1\*</sup>

- <sup>1</sup> Chemical and Biomolecular Engineering, Johns Hopkins University, Baltimore, MD 21218
- † Equal contributions
- \* Corresponding Author: tvo12@jhu.edu

#### **Data Availability and Reproducibility Statement**

Numerical data and results for structure and characterizations performed and shown in the main text are provided in the accompanying ZIP file with sample analysis scripts. Sample simulation scripts to perform both MC and MD simulations are included in the zip file. These analysis and simulation scripts will reproduce the data presented in all figures throughout the main text. We also provide sample simulation trajectory data (GSD file format) that represent the data/results that should come back from running the included files. All codes can also be found on our repository: <a href="https://github.com/VoGroupJHU/Anisotropic Chain.git">https://github.com/VoGroupJHU/Anisotropic Chain.git</a>.